ACADEMIC PRESS

Available online at www.sciencedirect.com
SCIENCE DIRECT®

Journal of Catalysis 217 (2003) 79–87

JOURNAL OF CATALYSIS

www.elsevier.com/locate/jcat

Ni/SiO_2 catalyst effective for methane decomposition into hydrogen and carbon nanofiber

Sakae Takenaka,* Shoji Kobayashi, Hitoshi Ogihara, and Kiyoshi Otsuka

Department of Applied Chemistry, Graduate School of Science and Engineering, Tokyo Institute of Technology, Ookayama, Meguro-ku, Tokyo 152-8552, Japan

Received 28 August 2002; revised 18 November 2002; accepted 2 December 2002

Abstract

Methane decomposition into hydrogen and carbon nanofibers was carried out over Ni/SiO_2. The catalytic activity of Ni/SiO_2 decreased with time on stream and finally the catalyst was deactivated completely. The initial catalytic activity and the yields of hydrogen and carbon nanofibers until complete deactivation of the catalysts depended strongly on the loading amount of Ni. The yield of carbon nanofibers reached the maximum (491 g_C/g_{Ni}) for Ni (40 wt%)/SiO_2, which is one of the highest values among those for catalysts reported so far. SEM images of the catalysts after methane decomposition suggested that the particle size of Ni metal controlled the yields of hydrogen and carbon nanofibers. The yields of hydrogen and carbon nanofibers also depended significantly on the reaction temperatures; i.e., the yields decreased sharply with a rise in the reaction temperatures at > 773 K. In addition, the reaction temperatures controlled the diameter and graphitic order of carbon nanofibers.

Keywords: Methane decomposition; Ni/SiO_2; Carbon nanofiber; CO-free hydrogen

1. Introduction

Hydrogen is a clean fuel in the sense that no CO_2 is emitted when it is used in H_2–O_2 fuel cells. The H_2–O_2 cells such as phosphoric acid and polymer electrolyte fuel cells require a thorough elimination of carbon monoxide (CO) from the fuel (H_2) because CO poisons strongly the electrocatalysts in the cells. At present, hydrogen is produced mainly through steam reforming and partial oxidation of natural gas. Because the hydrogen produced by these processes inevitably contains CO beyond a tolerable range, the removal of CO through a water gas shift reaction of CO followed by selective CO oxidation is required. This purification of CO inevitably adds extra cost and volume for the natural gas reformer.

Decomposition of methane into hydrogen and carbon is of current interest from a viewpoint of an alternative route of hydrogen production from natural gas [1,2]. Because no CO was contained in the products obtained by the methane decomposition, the hydrogen can be utilized directly as the fuel for H_2–O_2 cells. Recent studies have demonstrated clean hydrogen production via stepwise steam reforming of methane, i.e., decomposition of methane over supported Ni catalyst followed by steam gasification of surface carbon on the catalyst [3].

On the other hand, research in the field of carbon nanotubes and carbon nonofibers, which are coproduced in the catalytic methane decomposition, has undergone an explosive growth since the discovery of carbon nanotubes [4]. Due to the extraordinary property of carbon nanotubes and carbon nanofibers, several researchers have explored the use of the carbons for such applications as catalyst supports, adsorbents for hydrogen, and electrodes [5–7]. In addition, the carbon nanofiber showed a specific reactivity in their gasification with water and CO_2 [8,9]. The products, synthesis gas or CO, should be used in the chemical industry.

Concerning the catalysts for the decomposition of methane, it is well known that supported Ni is one of the effective catalysts [10–12]. Generally, the catalytic activity of supported Ni catalysts decreased with time on stream due to deposition of a large amount of carbons on the catalysts. Therefore, it is required to develop catalysts with a long life as well as high activity. Recently, preferential effects of the addition of other metals to supported Ni

* Corresponding author.
E-mail address: stakenak@o.cc.titech.ac.jp (S. Takenaka).

0021-9517/03/$ – see front matter
doi:10.1016/S0021-9517(02)00185-9

catalysts or the preparation methods of Ni-based catalysts such as coprecipitation or impregnation methods on the catalytic performance for methane decomposition have been examined [13,14]. We have already examined the effect of catalytic supports (MgO, Al_2O_3, SiO_2, TiO_2, ZrO_2, $MgO \cdot SiO_2$, $Al_2O_3 \cdot SiO_2$, H^+-ZSM-5, and so on) of Ni on the catalytic performance for methane decomposition and reported that silica is one of the most effective supports for the formation of hydrogen and carbon nanofibers among various supports [15]. Thus, we focus our attention on the silica-supported Ni catalyst in order to design a catalyst with a longer life and higher activity. In the present study, we carried out methane decomposition over silica-supported Ni catalysts under different conditions and investigated the factors which determined the catalytic activity and life for methane decomposition. In addition, the characterization of the carbon nanofibers formed at different temperatures was described.

2. Experimental

Ni/SiO_2 was prepared by impregnating SiO_2 (Kieselgel 100 from Merck, specific surface area = 250 $m^2\,g^{-1}$, pore volume = 1.1 $ml\,g^{-1}$) with an aqueous solution of $Ni(NO_3)_2 \cdot 6H_2O$, followed by a drying up the impregnated sample at 373 K for 12 h. The sample was dried at 573 K for 5 h and calcined at 873 K for 5 h under an air stream. Methane decomposition over the Ni/SiO_2 catalyst was carried out in a conventional gas-flow system. A Ni/SiO_2 catalyst powder (0.040 g) put at the bottom of a quartz reactor was treated under a stream of hydrogen at 823 K prior to methane decomposition. Methane decomposition was initiated by the contact of a stream of methane ($P(CH_4)$ = 101 kPa, flow rate = 60 $ml\,min^{-1}$) with the catalyst. During the methane decomposition, part of the stream gases of the catalyst bed was sampled and analyzed by G.C. Conversion of methane was evaluated from the amounts of hydrogen formed, assuming that the reaction, $CH_4 \rightarrow C + 2H_2$, proceeded selectively. In fact, hydrogen only was confirmed as a gaseous product during the reaction.

X-ray diffraction patterns were measured by a Rigaku RINT 2500V diffractometer using Cu-K_α radiation at room temperature.

Raman spectra were taken with the 514.5-nm line of an argon laser (JASCO NRS-2100) at room temperature. The incident laser power at the sample was 2 mW. The spectra were recorded with a resolution of 4 cm^{-1}.

X-ray absorption experiments were carried out on the beamline BL-9A at Photon Factory in the Institute of Materials Structure Science for High Energy Accelerator Research Organization, Tsukuba, Japan, with a ring energy of 2.5 GeV and a stored current of 250–450 mA (Proposal 2000G074). The X-ray absorption spectra of the catalysts were recorded in a fluorescence mode, and that of Ni foil was recorded in a transmission mode with a Si(111) two-crystal monochromator at room temperature. Normalization of XANES was performed as described elsewhere [16].

A SEM image and back-scattering electron image of the catalyst were measured using a Hitachi FE-SEM S-800 (field emission gun scanning electron microscope).

3. Results and discussion

Fig. 1 shows the changes in methane conversions with time on stream for the methane decomposition at 773 K over the Ni/SiO_2 catalysts with different loadings of Ni. The upper and lower figure parts show the change in methane conversion with time on stream from 0 to 1 h and 0 to 80 h, respectively. The loading amounts of Ni in the Ni/SiO_2 were changed from 1 to 90 wt%. Over all the catalysts, only hydrogen was detected as a gaseous product, i.e. the methane decomposition, $CH_4 \rightarrow 2H_2 + C$, proceeded selectively. Generally, the methane conversion was high just after the contact of methane with the catalysts and decreased rapidly or gradually with time on stream. Finally, all the catalysts were deactivated completely for the reaction. The initial catalytic activity and the time until complete deactivation of the catalyst (catalytic life) depended strongly on the loading of Ni metal. The time until complete deactivation of the catalysts increased on the order of 1 wt% (100 min) < 5 wt% (240 min) < 90 wt% (500 min) < 13 wt% (630 min) < 20 wt% (1380 min) < 70 wt% (1930 min) < 35 wt% (2760 min) < 50 wt% (3480 min) < 40 wt% (4320 min).

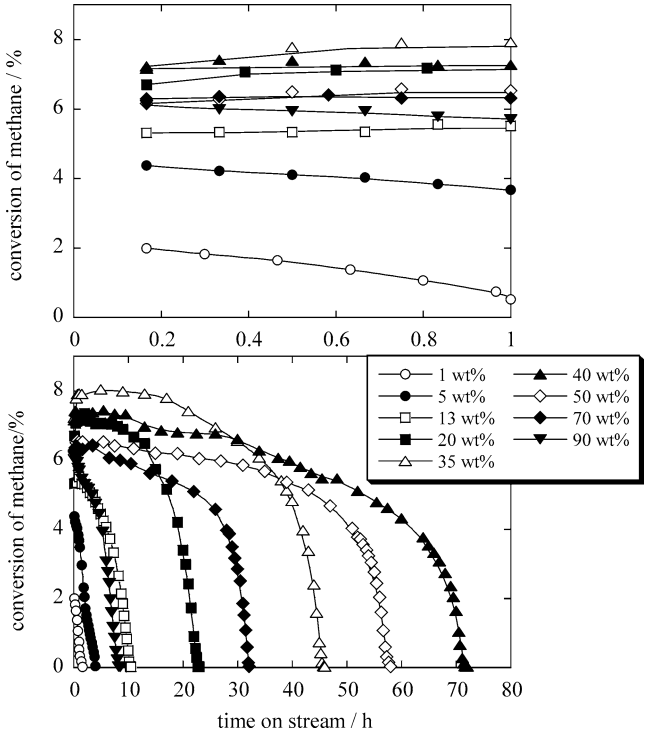

Fig. 1. Kinetic curves of methane conversions in the methane decomposition over Ni/SiO_2 catalysts at 773 K. Catalysts: 0.040 g methane; P = 101 kPa and flow rate = 60 $ml\,min^{-1}$.

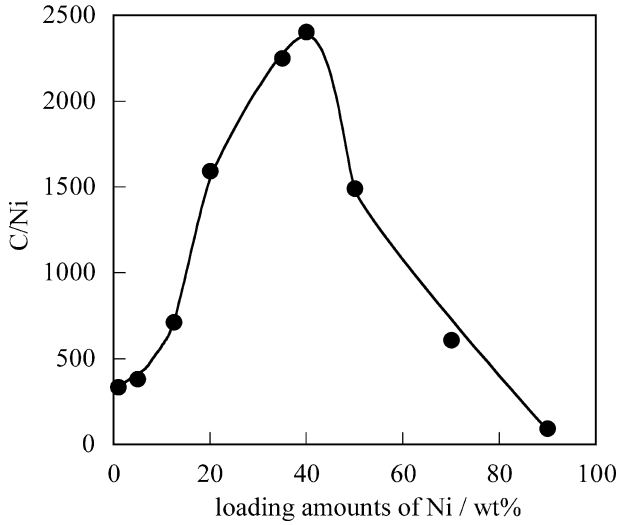

Fig. 2. Changes in the C/Ni value as a function of the loading amount of Ni in Ni/SiO_2 catalysts.

The initial catalytic activity became higher and catalytic life became longer with loading amounts of Ni in the range from 1 to 40 wt%. However, loading of Ni of more than 50 wt% caused decreases in the initial activity as well as catalytic life for methane decomposition.

Fig. 2 shows the carbon yields (C/Ni, defined as the number of methane molecules decomposed per one Ni atom in each Ni/SiO_2 catalyst) until the complete deactivation of the catalysts. The C/Ni value was evaluated from the results in Fig. 1, assuming that the decomposition, $CH_4 \rightarrow 2H_2 + C$, took place selectively. The C/Ni value (the amount of deposited carbons) was also evaluated from the weight of the catalyst which had been deactivated completely for methane decomposition. The value evaluated from the weight of the catalyst with deposited carbons was highly consistent with that from the amount of hydrogen formed. The C/Ni value increased remarkably as the loading amounts of Ni increased from 1 to 40 wt% and the value reached the maximum (C/Ni = 2403) at 40 wt% loading of Ni metal. When the loading amounts exceeded 40 wt%, the C/Ni values decreased sharply. The C/Ni value (= 2403) for Ni (40 wt%)/SiO_2 corresponded to 491 g of deposited carbon per 1 g of Ni in the catalyst. Recently, Ni-based catalysts with high activity for methane decomposition have been designed by some research groups. Avdeeva et al. reported methane decomposition over Ni/Al_2O_3, which was prepared by coprecipitating the components [17]. The highest yield of carbons was estimated to 161 g per 1 g of Ni when the loading amount of Ni was 90 wt%. Also, they reported the effects of the addition of a Cu ion to the Ni/Al_2O_3 catalyst on methane decomposition. Introduction of Cu at 3 wt% allowed the carbon yield to be improved to 276 g of deposited carbon per 1 g of Ni. Ermakova et al. investigated methane decomposition over a Ni/SiO_2 catalyst, which was prepared by impregnation of NiO with an alcohol solution of tetraethoxisilane [14]. The highest yield of carbon deposited from methane was 384 g per 1 g of Ni, when SiO_2 was added at 10 wt% into Ni metal. Taking these previous reports into consideration, the Ni (40 wt%)/SiO_2 in this work was one of the most effective catalysts for methane decomposition among the catalysts reported so far.

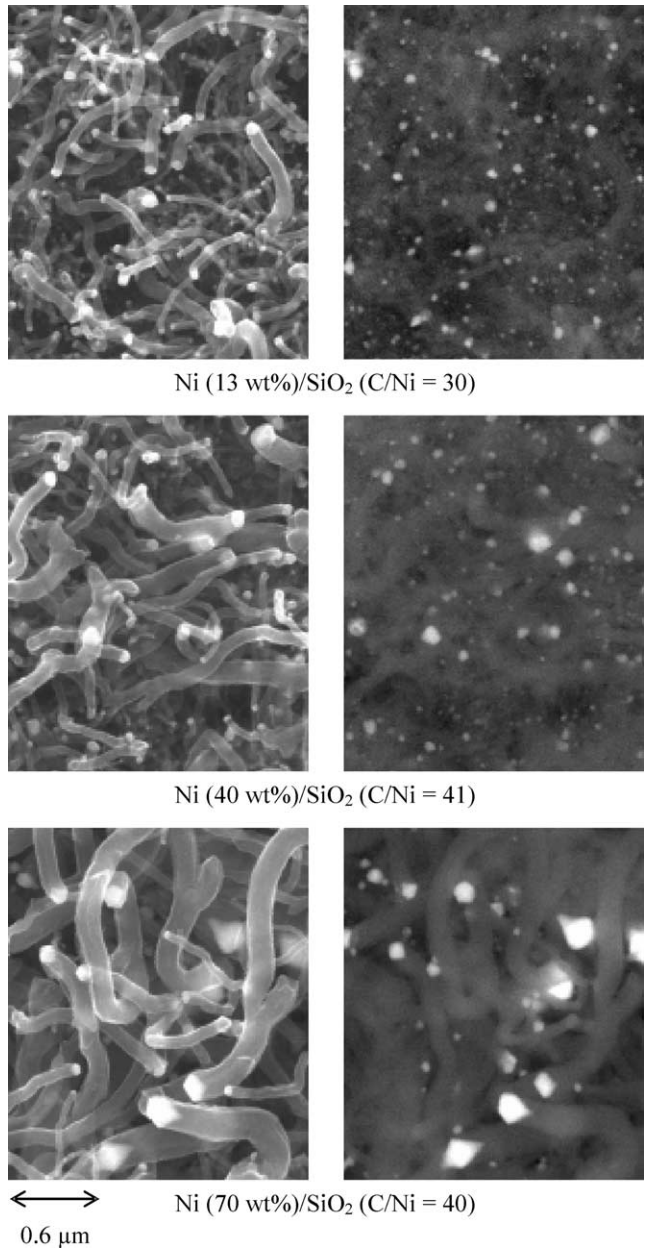

Fig. 3. SEM and back-scattering electron images of Ni/SiO_2 catalysts at the early period of methane decomposition (C/Ni = 30–41) at 773 K.

The catalytic performance of Ni/SiO_2 catalysts for methane decomposition depended strongly on the loading amount of Ni metal, suggesting that the catalytic performance could be related to the particle size of Ni metal. The SEM images and back-scattering electron images (BEI) suggested a correlation between the catalytic performance of the Ni/SiO_2 and the particle sizes of Ni metal. Figs. 3 and 4 show the SEM images and BEIs of the Ni/SiO_2 catalysts

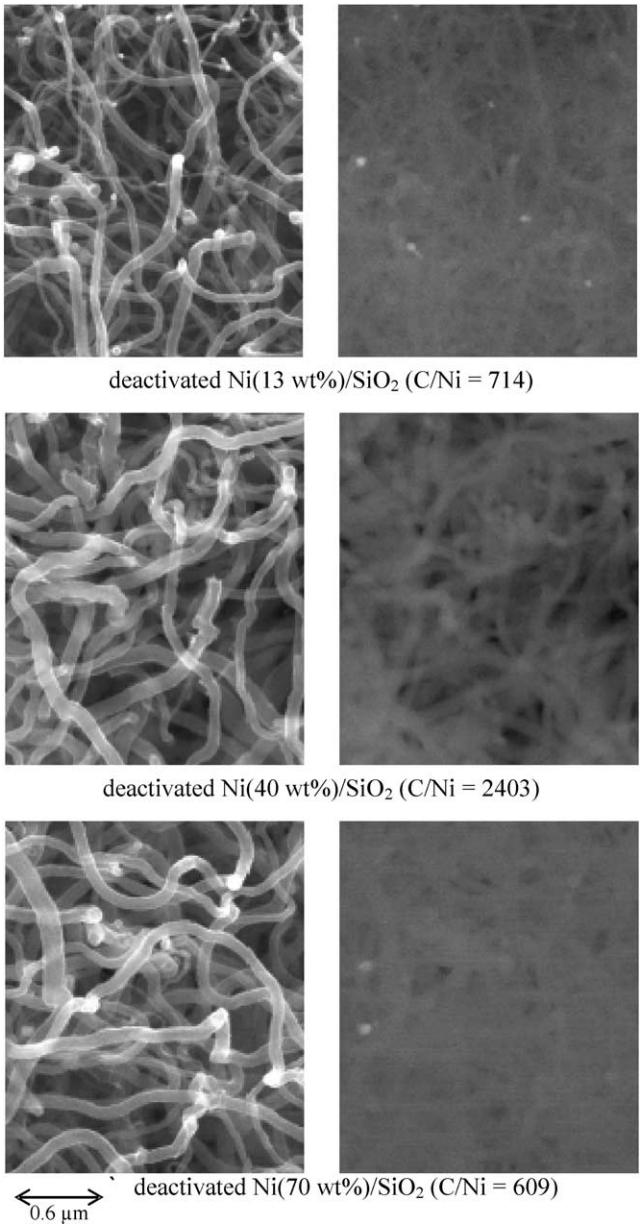

Fig. 4. SEM and back-scattering electron images of Ni/SiO_2 catalysts which had been deactivated completely by the methane decomposition at 773 K.

at an early period of methane decomposition ($C/Ni = 30$–41) and the images after complete deactivation, respectively. The methane decomposition was carried out at 773 K over the Ni/SiO_2 catalysts with Ni loading amounts of 13, 40, and 70 wt%. All the BEIs shown in Figs. 3 and 4 were measured at the same time as the corresponding SEM images. All the SEM images showed that the carbons deposited from methane decomposition grow with a filamentous structure. The bright spots in BEI, which indicate the position and size of Ni metal particles in this case, were located at the tips of carbon nanofibers observed in SEM images, and the diameters of the Ni metal particles were almost the same as that of the nanofiber. It is generally accepted that the

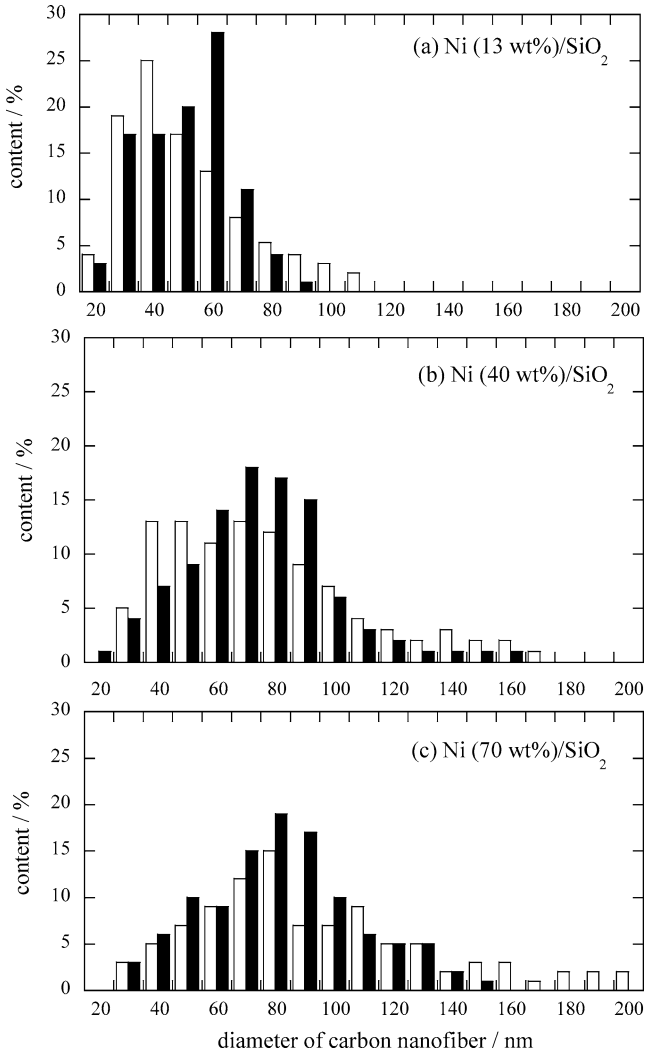

Fig. 5. Diameter distribution of carbon nanofibers formed by methane decomposition at 773 K over Ni/SiO_2. White bar: early period of methane decomposition ($C/Ni = 30$–41), black bar: after deactivation of the catalysts for methane decomposition.

surface of the Ni metal particle present on the tip of a carbon nanofiber adsorbs methane and decomposes it into carbon and hydrogen atoms to form carbon nanofibers [18].

Fig. 5 shows the diameter distribution of carbon nanofibers formed by methane decomposition at 773 K over Ni/SiO_2. The white and black bars correspond to the distribution of the diameters of carbon nanofibers observed by SEM images at early periods of methane decomposition ($C/Ni = 30$–41) and after complete deactivation of the catalysts, respectively. Early in methane decomposition, the diameters of carbon nanofibers were distributed widely, i.e., 20–110 nm for Ni (13 wt%)/SiO_2, 30–170 nm for Ni (40 wt%)/SiO_2, and 30–200 nm for Ni (70 wt%)/SiO_2. The fraction of the carbon nanofibers with larger diameters increased as the loading amount of Ni in the catalyst became higher. Early in methane decomposition, Ni metal particles decomposed methane irrespectively of the particle sizes to form carbon nanofibers with different diameters.

On the other hand, the diameters of carbon nanofibers observed in each SEM image of the deactivated Ni/SiO_2 (Fig. 4) were relatively uniform, in contrast with that of the early period of the reaction shown in Fig. 3. The diameter distribution of carbon nanofibers observed by SEM images of the deactivated catalysts is also shown in Fig. 5. The fraction of carbon nanofibers with diameters smaller than 40 nm for Ni (13 wt%)/SiO_2 and Ni (40 wt%)/SiO_2, and with diameters larger than 140 nm for Ni (40 wt%)/SiO_2 and Ni (70 wt%)/SiO_2, decreased after complete deactivation (black bar). Thus, the fraction of carbon nanofibers with diameters from 60 to 100 nm increased significantly after complete deactivation of the catalysts, irrespective of the loading amount of Ni metal. As methane decomposition proceeded over the Ni/SiO_2 catalyst, the surface of the catalyst was covered with carbon nanofibers, which inevitably deactivated the catalyst. Therefore, it is reasonable to consider that the SEM images of the deactivated catalysts showed the nanofibers formed at the latest stage of methane decomposition, i.e., the nanofibers formed by the Ni metal particles having the longest life. It is likely that the diameters of carbon nanofibers which can be seen in the SEM images of deactivated Ni/SiO_2 are uniform because Ni metal particles with a certain size (60–100 nm) show the longest catalytic life for methane decomposition.

The deactivation of catalysts for methane decomposition is accounted for by encapsulation of Ni metal particles at the tip of carbon nanofibers with deposited carbon [19,20]. During methane decomposition, methane is adsorbed and decomposed on a certain face of Ni metal; this process is followed by the diffusion of carbon atoms on the surface of catalytic particles and through the particles to precipitate at other faces in the form of a filament. The deactivation rate (catalytic life) is affected by diffusion in the nickel–carbon system and is determined by the ratio of formation rate of carbon atoms on the Ni metal surfaces by the methane decomposition to their diffusion rate approaching the deposite site. Thus, there is some optimal size of active Ni metal particles which remains in this equilibrium for the longest time [14,17]. As shown in Figs. 1 and 2, the carbon yield (C/Ni) became the highest when the Ni metal of 40 wt% was loaded on SiO_2. The result implies that the proportion of Ni metal particles with sizes from 60 to 100 nm is the highest for Ni (40 wt%)/SiO_2 among all the catalysts with different loading amounts. We have already reported that silica without a pore structure (Cab–O–Sil supplied from Cabot Co. specific surface area $= 200\ m^2\ g^{-1}$) was the most effective support among various silica supports when Ni metal was loaded with 5 wt% [15]. However, a smaller increase in carbon yields (C/Ni) was observed in the case of methane decomposition at 773 K over Ni/Cab–O–Sil compared to that for Ni/SiO_2 (Kieselgel) when the loading amount of Ni increased; i.e., C/Ni = 938, 1244, 1582, 1759, and 1646 for loading amounts of 5, 10, 20, 40, and 50 wt%, respectively. Therefore, the content of Ni metal particles with diameters from 60 to 100 nm would be lower for Ni (40 wt%)/Cab–O–Sil compared to Ni (40 wt%)/Kieselgel. It is likely that a pore structure of SiO_2 (Kieselgel) controls the particle sizes of Ni metal.

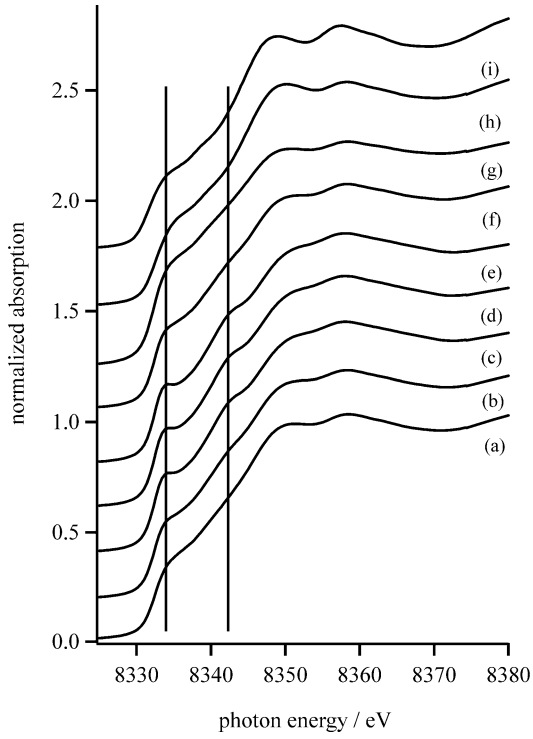

Fig. 6. Ni K-edge XANES spectra of Ni/SiO_2 catalysts deactivated completely for the methane decomposition at 773 K, a fresh Ni (5 wt%)/SiO_2 catalyst and a Ni foil. (a–g) deactivated Ni/SiO_2 catalysts with Ni loading of 5, 13, 20, 30, 40, 50, and 70 wt%, respectively; (h) a fresh Ni (5 wt%)/SiO_2 catalyst; (i) a Ni foil.

Fig. 6 shows Ni K-edge XANES spectra of Ni/SiO_2 catalysts deactivated completely for methane decomposition at 773 K, a fresh Ni (5 wt%)/SiO_2 catalyst (before contact of methane with the catalyst) and a Ni foil. The XANES spectrum of fresh Ni (5 wt%)/SiO_2 (h) was compatible with that of Ni foil (i). In addition, we confirmed that the XANES spectra of fresh Ni/SiO_2 catalysts with different loading amounts of Ni metal were quite similar to that of Ni foil. These results indicate that Ni species are present as Ni metal in the fresh Ni/SiO_2 catalysts. On the other hand, the XANES spectra of the Ni/SiO_2 changed after the complete deactivation for methane decomposition. In the XANES spectra of the deactivated Ni/SiO_2, the intensities of absorption at 8334 and 8343 eV became stronger and those at 8349 and 8358 eV became weaker, compared to those in the spectra of a Ni foil and a fresh Ni/SiO_2 catalyst. The change of XANES spectra was pronounced with a loading amount of Ni in the range from 5 to 40 wt%, where the carbon yield (C/Ni value) became higher as found in Fig. 2. We have already reported that the changes in XANES spectra of Ni/SiO_2 during the deactivation for methane decomposition, that is, appearance of the peaks at 8334 and 8343 eV and weakening of the peaks at 8349 and 8358 eV, were brought about by the change of Ni metal

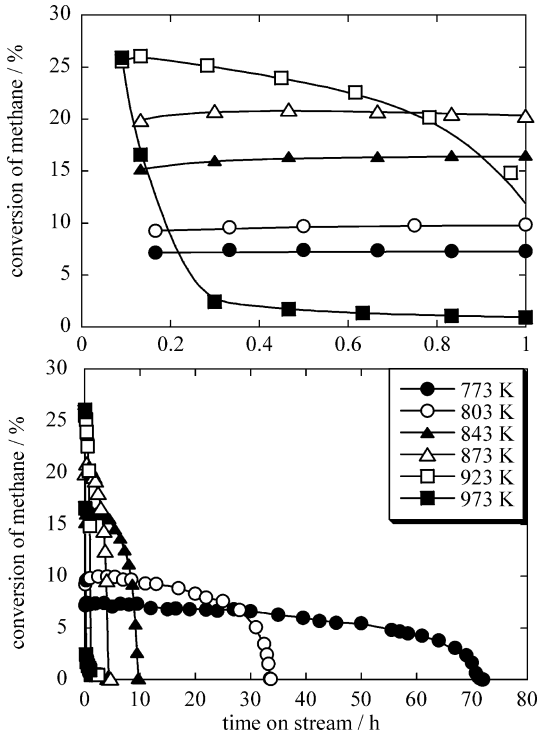

Fig. 7. Kinetic curves of methane conversions in the methane decomposition over Ni (40 wt%)/SiO_2 at different temperatures. Catalyst: 0.040 g methane; $P = 101$ kPa and flow rate $= 60$ ml min^{-1}.

to some Ni carbide species [21]. These results shown in Fig. 6 implied that the proportion of Ni carbide species to all the Ni species in the deactivated Ni/SiO_2 catalysts became higher as the carbon yield until complete deactivation of the catalysts became higher. The results of SEM and BEI described above suggested that the particle size of Ni metal determined the yields of hydrogen and carbon nanofibers in methane decomposition. It is likely that Ni metal with size suitable for methane decomposition is changed to some Ni carbide species during the deactivation of the catalyst. At the moment, we cannot explain why the Ni metal particles with longer life tend to change to some nickel carbide species during the deactivation.

Next, we investigated the effect of reaction temperatures on the catalytic performance of Ni (40 wt%)/SiO_2, which was the most active catalyst for methane decomposition at 773 K as described earlier. Fig. 7 shows the kinetic curves of methane conversion in the methane decomposition over Ni (40 wt%)/SiO_2 catalyst at different temperatures. The temperatures were changed from 773 to 973 K. Upper and lower parts of Fig. 7 depict the kinetic curves of methane conversion at time on stream from 0 to 60 min and 0 to 80 h, respectively. As the reaction temperatures became higher from 773 to 923 K, the conversion at ca. 10 min of the time on stream (the first plot) increased from 7 to 25%. On the other hand, the time until the complete deactivation of the catalyst became longer as the reaction temperature decreased. Fig. 8 shows the change in carbon yield (C/Ni) as a function of reaction temperature. The C/Ni values were estimated from

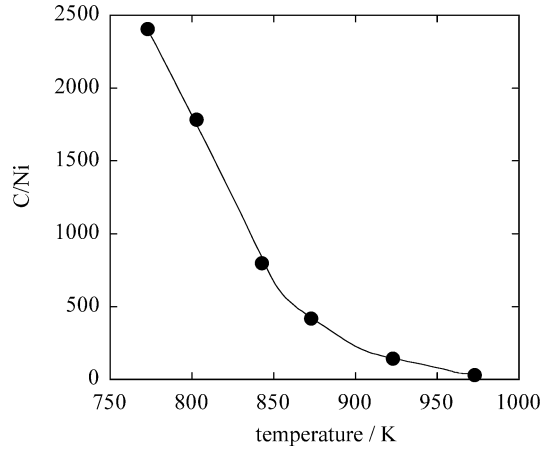

Fig. 8. Changes in the C/Ni value until the complete deactivation of the Ni (40 wt%)/SiO_2 catalyst as a function of reaction temperatures.

the results shown in Fig. 7 at the complete deactivation of Ni (40 wt%)/SiO_2. As the reaction temperature became higher, the C/Ni value decreased significantly. In particular, only a very small formation of hydrogen and carbon nanofibers was observed at 973 K (C/Ni = 29). These results indicate that lower reaction temperatures are needed in order to get high yields of hydrogen and carbon nanofibers in methane decomposition.

Fig. 9 shows the SEM images and BEIs of Ni (40 wt%)/SiO_2 catalysts after complete deactivation at 843, 923, and 973 K. The images of Ni (40 wt%)/SiO_2 deactivated at 773 K were shown in Fig. 4. All the SEM images show the presence of carbon nanofibers. The average diameters of carbon nanofibers formed at 843, 923, and 973 K were estimated to be ca. 60, 40, and 20 nm, respectively, indicating that the diameters of carbon nanofibers became smaller with a rise of reaction temperature. The BEI of catalyst deactivated at 973 K showed that many Ni metal particles are present in the visible field. However, most of the Ni metal particles observable were not located at the tip of nanofibers, i.e., the Ni metal particles did not form the nanofiber. As described earlier, the diameter of a carbon nanofiber was almost the same as that of the Ni metal particle present at the tip of the nanofiber. It is likely that Ni metal particles with smaller diameters are effective for the methane decomposition into carbon nanofibers as the reaction temperatures become higher.

Figs. 10 and 11 show the TEM images of carbon nanofibers formed by methane decomposition over Ni (40 wt%)/SiO_2 at 773 and 973 K, respectively. In the TEM images of the catalyst after the methane decomposition at 773 K shown in Fig. 10, the carbon nanofibers with diameters from 40 to 110 nm were observed. In addition, the graphene layers in the nanofiber are canted with respect to the longitudinal axis of the fibers (fish-bone type carbon fiber), and the Ni metal particle present at the tip of the carbon nanofiber is pear-shaped, which has been reported by many researchers [22–24]. On the other hand, the TEM images of catalyst after methane decomposition at 973 K (Fig. 11) show that the

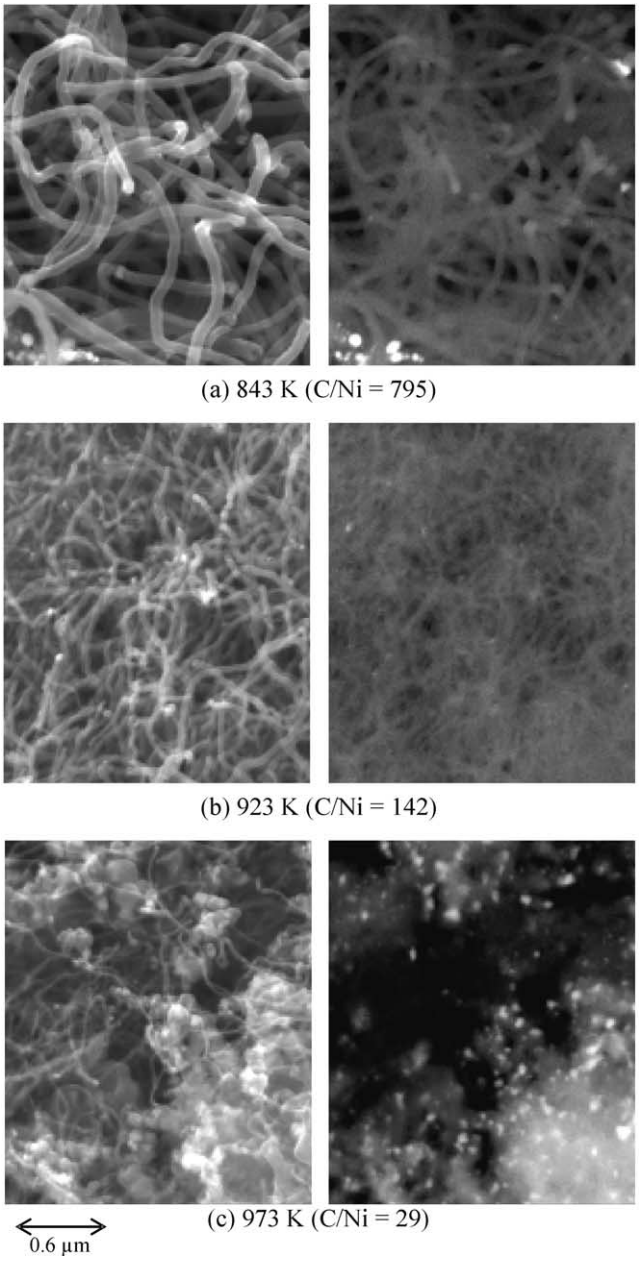

Fig. 9. SEM images and back-scattering electron images of the Ni (40 wt%)/SiO_2 catalysts which were deactivated by the methane decomposition at different temperatures.

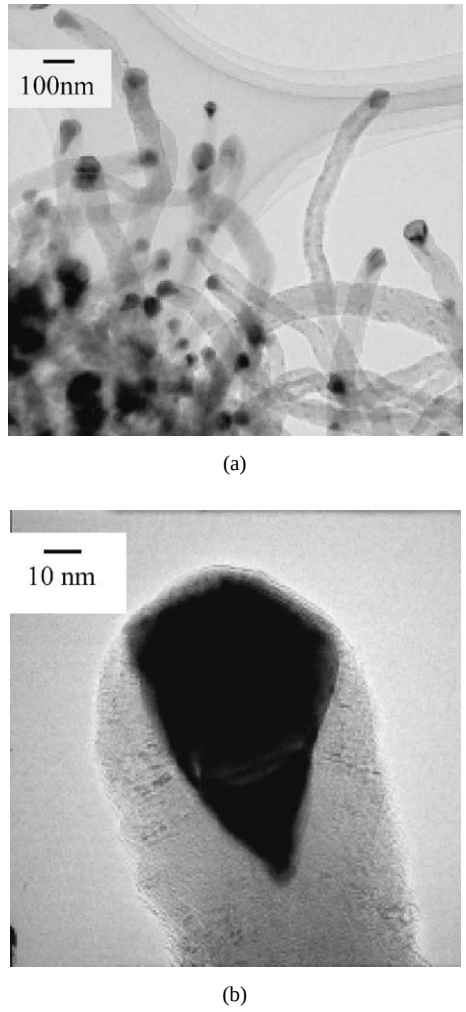

Fig. 10. TEM images of the carbons formed by methane decomposition over Ni (40 wt%)/SiO_2 at 773 K.

carbon nanotubes with diameters of ca. 20 nm are formed and graphene layers in the nanotubes are aligned along the fiber axis (multiwalled carbon nanotube). The shape of Ni metal particles present at the tip of the carbon nanotube formed at 973 K is almost spherical. In the methane decomposition over Ni/SiO_2 catalyst, carbon nanofibers and carbon nanotubes were formed by formation of carbon atoms from methane on the surface of Ni metal particles, the process being followed by the diffusion of carbon atoms on the metal surface and through the metal particle. We consider that carbon nanotubes were formed through the diffusion of carbon atoms on the surface of Ni metal particles mainly to form hollow structures, while the carbon nanofibers (fishbone type) were formed by the diffusion of carbon atoms through the Ni metal particles. The diffusion of carbon atoms on the surface of Ni metal particles may be preferential compared to that through the metal particles as reaction temperatures become higher.

Fig. 12 shows the Raman spectra of carbons deposited by methane decomposition at different temperatures over Ni (40 wt%)/SiO_2 catalyst. For all the Raman spectra, two bands were observed at ca. 1350 cm^{-1} (D band) and 1580 cm^{-1} (G band). The G band can be attributed to the in-plane carbon–carbon stretching vibrations of graphite layers and the D band is ascribed to the structural imperfection of graphite [25,26]. In addition, a shoulder peak in G band was found at ca. 1605 cm^{-1}. This shoulder band (denoted as D′ band) was reported to be assignable to the imperfect graphite or disordered carbons [27]. From the Raman spectra in Fig. 12, it was found that the relative intensity of the D band decreased and that of the G band increased as temperatures of methane decomposition became higher. The ratio of the area of the D band to that of the G band (I_D/I_G) can

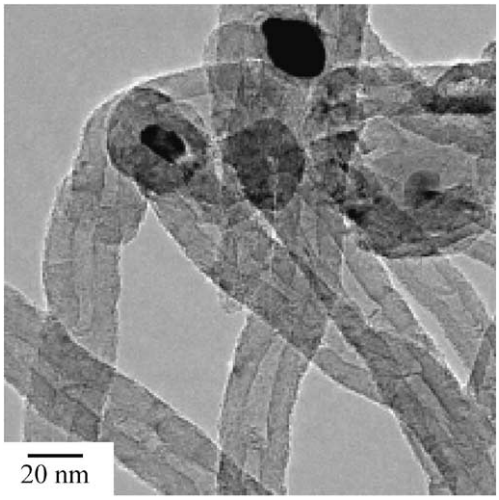

(a)

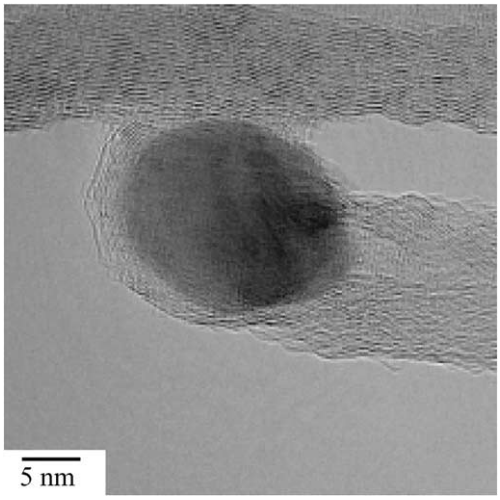

(b)

Fig. 11. TEM images of the carbons formed by methane decomposition over Ni (40 wt%)/SiO_2 at 973 K.

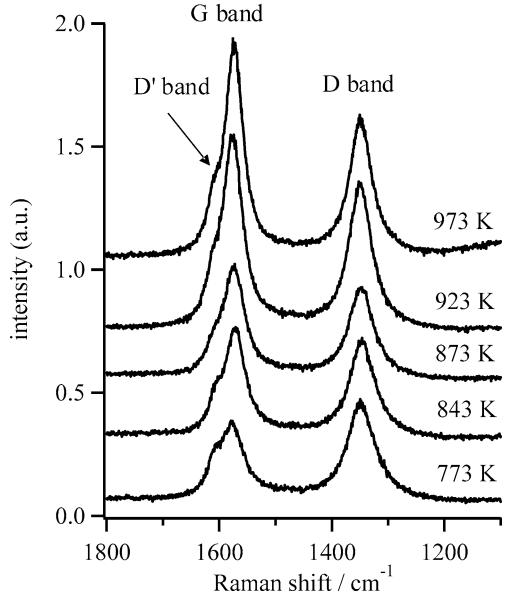

Fig. 12. Raman spectra of the carbons deposited by the methane decomposition over the Ni (40 wt%)/SiO_2 at different temperatures.

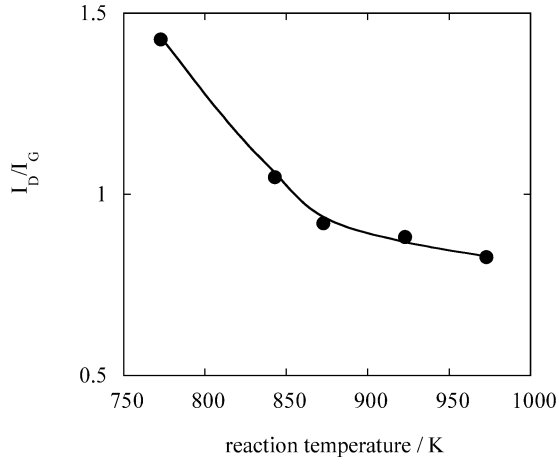

Fig. 13. Changes in the ratio (I_D/I_G) of area of the D band to that of the G band in Raman spectra of carbon nanofibers as a function of reaction temperatures.

be regarded as an index for the crystalline order of graphite [28–30]. Thus, we performed the curve fitting of each Raman spectrum shown in Fig. 12 using three Lorentzian lines for three bands (D, D′, and G band) to estimate the value of I_D/I_G. The results are shown in Fig. 13. The I_D/I_G value decreased with reaction temperature, indicating that the graphitic order of carbon nanofiber became higher with a rise in reaction temperatures. As shown in the TEM images (Figs. 10 and 11), multiwalled carbon nanotubes were formed in the decomposition of methane at 973 K, while the fish-bone type fibers were formed at low temperatures (773 K). Thus, the improvement of graphitic order shown by Raman spectra in Figs. 12 and 13 would be due to the formation of multiwalled carbon nanotubes at higher temperature, because the graphitic order of multiwalled carbon nanotubes was higher than that of the fish-bone type fibers.

4. Conclusion

We concluded as follows on the basis of the results described.

1. Ni (40 wt%)/SiO_2 is one of the most effective catalysts for methane decomposition among catalysts examined so for. The catalyst yields carbon nanofibers of 491 g per 1 g of Ni.
2. The catalytic life of Ni/SiO_2 for methane decomposition is related to the particle size of the Ni metal.
3. Yields of hydrogen and carbon nanofibers decreased significantly with the rise of reaction temperatures of methane decomposition. In the methane decomposition over Ni/SiO_2 at 773 K, fish-bone type carbon nanofibers

were formed, while at 973 K the multiwalled carbon nanotube was formed.

References

[1] Anonymous, Chem. Eng. 69 (1962) 90.
[2] N.Z. Muradov, Int. J. Hydrogen. Energy 18 (1993) 211.
[3] T.V. Choudhary, D.W. Goodman, J. Catal. 192 (2000) 316.
[4] S. Iijima, Nature 354 (1991) 56.
[5] K.P. de Jong, J.W. Geus, Catal. Rev.-Sci. Eng. 42 (2000) 481.
[6] A. Chambers, T. Nemes, N.M. Rodriguez, R.T.K. Baker, J. Phys. Chem. B 102 (1998) 2251.
[7] Sh.K. Shaikhutdinov, L.B. Avdeeva, B.N. Novgorodov, V.I. Zaikovskii, D.I. Kochubey, Catal. Lett. 47 (1997) 35.
[8] R. Aiello, J.E. Fiscus, H.-C. zur Loye, M.D. Amiridis, Appl. Catal. A 192 (2000) 227.
[9] S. Takenaka, K. Otsuka, Chem. Lett. 218 (2001).
[10] T. Ishihara, Y. Miyashita, H. Iseda, Y. Takita, Chem. Lett. 93 (1995).
[11] T.V. Choudhary, C. Sivadinarayana, C.C. Chusuei, A. Klinghoffer, D.W. Goodman, J. Catal. 199 (2001) 9.
[12] K. Otsuka, S. Kobayashi, S. Takenaka, Appl. Catal. A 190 (2000) 261.
[13] S.K. Shiakhutdinov, L.B. Avdeeva, O.V. Goncharova, D.I. Kochubey, B.N. Novgorodov, L.M. Plyasova, Appl. Catal. A 126 (1995) 125.
[14] M.A. Ermakova, D.Yu. Ermakov, G.G. Kuvshinov, L.M. Plyasova, J. Catal. 187 (1999) 77.
[15] S. Takenaka, H. Ogihara, I. Yamanaka, K. Otsuka, Appl. Catal. A 217 (2001) 101.
[16] S. Yoshida, S. Takenaka, T. Tanaka, H. Hirano, H. Hayashi, Stud. Surf. Sci. Catal. 101 (1996) 871.
[17] L.B. Avdeeva, O.V. Goncharova, D.I. Kochubey, V.I. Zaikovskii, L.M. Plyasova, B.N. Novgorodov, Sh.K. Shaikhutdinov, Appl. Catal. A 141 (1996) 117.
[18] R.T.K. Baker, Carbon 27 (1989) 315.
[19] E.G.M. Kuijpers, R.B. Tjepkema, J.W. Geus, J. Mol. Catal. 25 (1984) 241.
[20] G.G. Tibbetts, M.G. Devour, E.J. Rodda, Carbon 25 (1987) 367.
[21] S. Takenaka, H. Ogihara, K. Otsuka, J. Catal. 208 (2002) 54.
[22] R.T.K. Baker, M.A. Barber, P.S. Harris, F.S. Feates, R.J. Waite, J. Catal. 26 (1972) 51.
[23] P.A. Tesner, E.Y. Rovinovich, I.S. Rafalkes, E.F. Arefieva, Carbon 8 (1970) 435.
[24] T. Baird, J.R. Fryer, B. Grant, Carbon 12 (1974) 591.
[25] K. Sinha, J. Menendez, Phys. Rev. B 41 (1990) 10845.
[26] R.J. Nemanich, S.A. Solin, Phys. Rev. B 20 (1979) 392.
[27] H. Darmstadt, L. Sümmchen, J.-M. Ting, U. Roland, S. Kaliaguine, C. Roy, Carbon 35 (1997) 1581.
[28] R.O. Dilion, J.A. Woollam, V. Katkanant, Rhys. Rev. B 29 (1984) 3482.
[29] T. Jawhari, A. Roid, J. Casado, Carbon 33 (1995) 1561.
[30] A. Cuesta, P. Dhamelincourt, J. Laureyns, A. Martinez-Alonso, J.M.D. Tascon, Carbon 32 (1994) 1523.